Meteoritics & Planetary Science 41, Nr 1, 49–65 (2006)
Abstract available online at http://meteoritics.org

Maximal size of chondrules in shock wave heating model: Stripping of liquid surface in a hypersonic rarefied gas flow

Takaaki KATO[1, 2], Taishi NAKAMOTO[3*], and Hitoshi MIURA[1, 4]

[1]Pure and Applied Sciences, University of Tsukuba, Tsukuba, Japan
[2]NEC Aerospace Systems, Ltd., Yokohama, Japan
[3]Center for Computational Sciences, University of Tsukuba, Tsukuba, Japan
[4]Research Fellow of the Japan Society for the Promotion of Science
[*]Corresponding author. E-mail: nakamoto@ccs.tsukuba.ac.jp

(Received 31 January 2005; revision accepted 31 December 2005)

Abstract–We examined partially molten dust particles that have a solid core and a surrounding liquid mantle, and estimated the maximal size of chondrules in a framework of the shock wave heating model for chondrule formation. First, we examined the dynamics of the liquid mantle by analytically solving the hydrodynamics equations for a core-mantle structure via a linear approximation. We obtained the deformation, internal flow, pressure distribution in the liquid mantle, and the force acting on the solid core. Using these results, we estimated conditions in which liquid mantle is stripped off from the solid core. We found that when the particle radius is larger than about 1–2 mm, the stripping is expected to take place before the entire dust particle melts. So chondrules larger than about 1–2 mm are not likely to be formed by the shock wave heating mechanism. Also, we found that the stripping of the liquid mantle is more likely to occur than the fission of totally molten particles. Therefore, the maximal size of chondrules may be determined by the stripping of the liquid mantle from the partially molten dust particles in the shock waves. This maximal size is consistent with the sizes of natural chondrules.

INTRODUCTION

Most meteorites falling on the Earth are chondritic meteorites. Chondrules, which are ferromagnesian silicates, are a major component of chondritic meteorites. It is thought that chondrules were formed in the solar nebula about 4.6×10^9 years ago (e.g., Jones et al. 2000 and references therein), so we may obtain unique information about the solar nebula through the investigation of chondrules. From mineralogical features, it is thought that chondrules were formed through melting at least once and re-solidifying with rapid cooling. One prominent feature of chondrules is that they have a characteristic size distribution: diameters of most of chondrules are in a range from 0.1 mm to 1 mm (some chondrules have sizes out of this range, but they are uncommon). Many formation models for chondrules have been proposed to date, but none has been widely accepted. Any formation model for chondrules must be consistent with the size distribution.

The shock wave heating model is a plausible model for chondrule formation, since many chondrule features appear to be explained by it (e.g., Boss 1996; Connolly and Love 1998; Jones et al. 2000, and references within). When a shock wave is generated in the solar nebula, the relative velocity between dust particles and the gas flow can lead to frictional heating of the particles. When the particle melts due to the shock wave heating, deformation of and internal flow in the molten particle may be driven by a hypersonic rarefied gas flow around the molten particle. For a completely molten particle, linearized hydrodynamics equations have been used to obtain the deformation, internal flow, and pressure distribution in the molten particle (Sekiya et al. 2003). Also, the possible maximal size of chondrules was estimated based on the balance between the ram pressure of the hypersonic gas flow and the surface tension of the liquid sphere (Susa and Nakamoto 2002). These results are consistent with the sizes of natural chondrules.

Typically, in shock wave heating models the temperature in a particle is assumed to be uniform. However, when the time scale of heat conduction in a particle is longer than the time scale of melting, the particle will gradually melt from the surface to the center and a partial melting state will be obtained. So a dust particle that has a central solid core surrounded by a liquid mantle may be obtained. If this is the

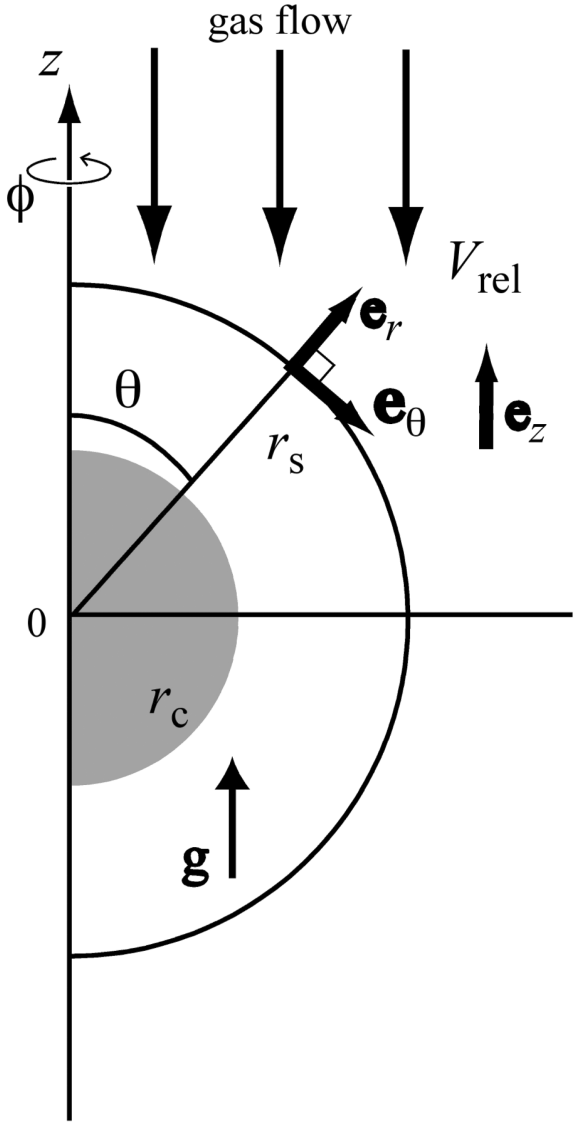

Fig. 1. A schematic view of the set-up. A solid core (gray) of radius r_c is surrounded by a liquid mantle (white) of radius r_s. Axisymmetry is assumed and the polar coordinates are employed. Gas molecules flow from upward (+z) to downward (–z). The apparent gravitational acceleration g emerges toward the +z direction due to the deceleration of the dust particle.

case, the dynamical stability of the dust particle with the liquid surface and the solid core against the hypersonic gas flow could be different from that of the completely molten particle, so the stability should be examined to, hopefully, reveal something about the formation process of chondrules.

In this study, first we obtain the flow in the liquid mantle. But it is not easy to solve a general situation, so we employ a lot of assumptions to simplify the problem. We assume that the flow is axisymmetric and steady, the solid core and liquid mantle are concentric, physical properties such as the density, the viscosity, and the conductivity are spatially and temporally constant, the deformation is small, and so forth. Thanks to these simplifications, we can analytically solve linearized hydrodynamics equations for particles with a core-mantle structure. And we obtain the deformation, internal flow, pressure distribution in the liquid mantle, and the force acting on the solid core. Although we know that these simplifications are not realistic and the real chondrule cases should be much complicated, we still think that it is worth obtaining such an analytic solution of the liquid mantle behavior to investigate the chondrule formation process. It may give us a basic and insightful solution. And it enables us to use the analytic solution as a base of realistic and complicated non-linear numerical solutions in the future. The analytic solution is the first main result of this study.

Second, applying the obtained solution, we roughly estimate the time scale such that the solid core would separate from the liquid mantle due to the drag force. This phenomenon can be regarded as the stripping of the liquid mantle from the solid core. When stripping takes place, it leads to a reduction in particle size. This may determine the maximal size of chondrules formed by the shock wave heating process. We discuss this possibility by evaluating different time scales: heating, conduction, and the dynamical time scales. Also, we compare the effect of stripping from a partially molten particle and the fission of the completely molten particle to the maximal size of chondrules. We find that the maximal size of chondrules is likely to be determined by the stripping.

MODEL

In this study, we examine the dynamical properties of a partially molten particle. For that purpose, we discuss a situation where a central solid core is surrounded by a liquid spherical mantle. We assume that the liquid mantle does not evaporate, the densities of solid and liquid material are the same, and the volume is constant. (We discuss a case where the density of solid is different from liquid in section Porous Particle Case). Although, in reality, the temperature, material density, and viscosity of the liquid mantle may change, we assume that they are spatially and temporally constant. We also assume that the time scale of the deceleration is much longer than the dynamical and thermal conduction time scales within the liquid mantle (the validity of this assumption will be discussed in section Stripping). Then the internal flow, pressure distribution, and deformation of the surface are obtained by solving steady state fluid equations. We use the spherical co-ordinate system (r, θ, ϕ). A hypersonic rarefied gas flows downward along the z-axis with the velocity v_{rel} (Fig. 1). The gas flow is approximated by the free molecular flow, because the velocity of the flow is faster than the sound velocity of the gas and the mean free path is larger than the size of the dust particle. It is also assumed that the flow in the liquid shell is axisymmetric with respect to the z-axis, so $\partial / \partial \phi = 0$, and the flow has no azimuthal component of the

velocity, i.e., $\upsilon_\phi = 0$. The central solid core is a sphere with radius r_c and the shape is supposed not to be deformed. The radius of the outer liquid mantle is given by r_s. Strictly speaking, the liquid mantle is not a spherical shell with a constant outer radius, but is somewhat deformed. We choose the origin of the spherical co-ordinates so that $dr_s/d\theta = 0$ at $\theta = \pi/2$ as shown in Fig. 1. The unit vectors in r, θ, and ϕ directions are denoted by $\mathbf{e}_r$, $\mathbf{e}_\theta$, and $\mathbf{e}_\phi$, respectively. The position vector on the surface of the sphere is written by $\mathbf{r}_s = r_s\mathbf{e}_r$.

The boundary condition for the flow in the liquid mantle on the surface of the central solid core is given by:

$$\mathbf{v} = 0 \tag{1}$$

where $\mathbf{v} = \upsilon_r\mathbf{e}_r + \upsilon_\theta\mathbf{e}_\theta$ is the fluid velocity in the liquid mantle. The boundary condition on the surface of the liquid sphere is given by:

$$\mathbf{v} \cdot \mathbf{n} = 0 \tag{2}$$

where $\mathbf{n} = (n_r, n_\theta, n_\phi)$ is the unit normal vector of the surface (Fig. 2). Since the particle shape is assumed to be axisymmetric, $n_\phi = 0$.

From the balance of forces among the ram pressure by the gas flow, the surface tension, and the stress tensor on the surface, we have (Appendix A):

$$-(\mathbf{n}\cdot\mathbf{e}_z)p_{fm}H[\pi/2-\theta]\mathbf{e}_z = n_r\sigma_{rr}\mathbf{e}_r + n_\theta\sigma_{\theta r}\mathbf{e}_r + n_r\sigma_{r\theta}\mathbf{e}_\theta + n_\theta\sigma_{\theta\theta}\mathbf{e}_\theta + T_s\left(\frac{1}{R_\theta}+\frac{1}{R_\phi}\right)\mathbf{n} \tag{3}$$

The continuity and the Navier-Stokes equations of the flow in the liquid mantle are given by (e.g., Landau and Lifshitz 1987):

$$r\frac{\partial \upsilon_r}{\partial r} + 2\upsilon_r + \frac{\partial \upsilon_\theta}{\partial \theta} + \upsilon_\theta\cot\theta = 0 \tag{4}$$

$$\upsilon_r\frac{\partial \upsilon_r}{\partial r} + \frac{\upsilon_\theta}{r}\frac{\partial \upsilon_r}{\partial \theta} - \frac{\upsilon_\theta^2}{r} = g\cos\theta - \frac{1}{\rho}\frac{\partial p}{\partial r} + \frac{\eta}{\rho}\left[\frac{\partial^2\upsilon_r}{\partial r^2} + \frac{4}{r}\frac{\partial \upsilon_r}{\partial r} + \frac{2\upsilon_r}{r^2} + \frac{1}{r^2}\left(\frac{\partial^2\upsilon_r}{\partial\theta^2} + \cot\theta\frac{\partial\upsilon_r}{\partial\theta}\right)\right] \tag{5}$$

$$\upsilon_r\frac{\partial \upsilon_\theta}{\partial r} + \frac{\upsilon_\theta}{r}\frac{\partial \upsilon_\theta}{\partial \theta} + \frac{\upsilon_r\upsilon_\theta}{r} = -g\sin\theta - \frac{1}{\rho r}\frac{\partial p}{\partial\theta} + \frac{\eta}{\rho}\left(\frac{\partial^2\upsilon_\theta}{\partial r^2} + \frac{2}{r}\frac{\partial\upsilon_\theta}{\partial r} - \frac{1}{r}\frac{\partial^2\upsilon_r}{\partial\theta\partial r}\right) \tag{6}$$

where ρ is the density of the liquid mantle and g is the apparent gravitational acceleration given below. Usual form of the Navier-Stokes equations have been transformed into Equations 5 and 6 by using Equation 4. In our co-ordinate system, which is co-moving with the center of mass, apparent gravitational acceleration g emerges, which is given by:

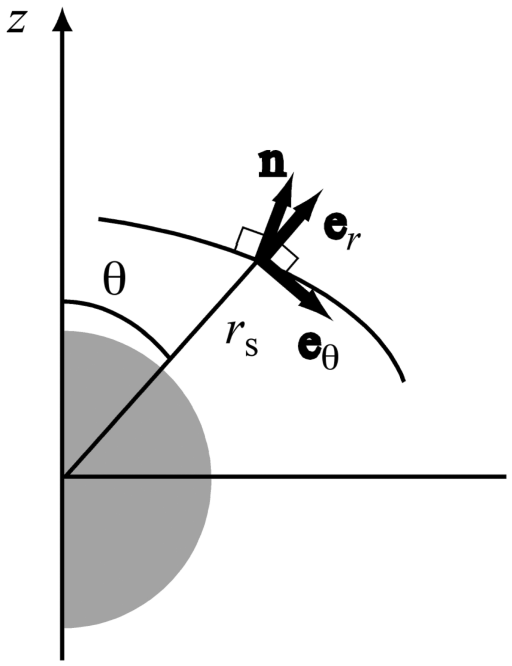

Fig. 2. Geometry of the liquid surface. The liquid surface can be deformed. Unit vectors in r and θ directions are $\mathbf{e}_r$ and $\mathbf{e}_\theta$, and the unit normal vector of the surface is $\mathbf{n}$, respectively.

$$g = \frac{\pi(r_{s|\theta=\pi/2})^2 p_{fm}}{V\rho} \tag{7}$$

where V is the volume of the particle.

We assume that the densities of solid and liquid materials in the particle are both $\rho = 3.0 \times 10^3$ kg m^{-3} and the viscosity of the liquid mantle η is $\eta = 0.2$ Pa · s (Uesugi et al. 2003). Although the viscosity can strongly depend on the temperature and the chemical composition, we assume that it is spatially and temporally constant for simplicity. In our simplified model, when the temperature of a point just above the solid core is not high enough and the viscosity at the point is quite high, that point may be regarded as a part of the solid core. Detailed analyses of more realistic and complicated situations should be done in the future, but they are beyond the scope of the present study. We also assume that the surface tension coefficient is similar to that of the molten basalt, so we adopt $T_s = 0.4$ N m^{-1} (Murase and McBirney 1973).

SOLUTION OF LINEARIZED EQUATIONS

Linear Approximation and Non-Dimensional Variables

We can obtain the flow in the shell and its deformation by solving the hydrodynamics equations with the boundary conditions written in Equations 1, 2, and 3. But it is somewhat a complicated problem to solve these equations in a non-linear regime. In this study, we merely solve them with a linear approximation for steady flow. The applicability of

linear solutions will be discussed in section Applicability of Linear Solution. In the following, we denote the unperturbed and perturbed quantities by subscript 0 and 1, respectively. For the unperturbed state with $p_{fm} = 0$, we have $g_0 = \upsilon_{r0} = \upsilon_{\theta 0}$, $\partial\upsilon_r/\partial r = \partial\upsilon_\theta/\partial r = \partial\upsilon_r/\partial\theta = \partial\upsilon_\theta/\partial\theta = 0$, and the radius of the sphere is given by $r_{s0} = (3V/4\pi)^{1/3}$. From Equation 3, we have the well-known equation:

$$p_0 = 2T_s/r_{s0} \tag{8}$$

For perturbed state with $p_{fm1} = \rho_{gas}\upsilon_{\mathrm{rel}}^2$, we assume that the deformation, which is defined by $r_{s1} = r_s - r_{s0}$, is much smaller than the unperturbed radius, i.e., $|r_{s1}| \ll r_{s0}$, and the nonlinear terms, i.e., all the terms on the left-hand side of Equations 5 and 6, are negligible (the validity of this assumption will be discussed in section Applicability of Linear Solution). The apparent gravitational acceleration is a first order quantity and is given from Equation 7 as:

$$g_1 = \frac{3p_{fm1}}{4\rho r_{s0}} \tag{9}$$

by neglecting higher order terms. Using these conditions, we solve the linearized equations (see Appendix C).

In the course of solving the equations, we use the following non-dimensional variables:

$$x \equiv r/r_{s0} \tag{10}$$

$$x_c \equiv r_c/r_{s0} \tag{11}$$

$$\Psi \equiv p_1/p_{fm1} \tag{12}$$

$$u \equiv \eta\upsilon_{r1}/(p_{fm1}r_{s0}) \tag{13}$$

$$w \equiv \eta\int_0^\theta \upsilon_{\theta 1}d\theta/(p_{fm1}r_{s0}) \tag{14}$$

and

$$x_s \equiv T_s r_{s1}/(p_{fm1}r_{s0}^2) \tag{15}$$

From Equation 14, we have:

$$\upsilon_{\theta 1} = \frac{p_{fm1}r_{s0}}{\eta}\frac{\partial w}{\partial\theta} \tag{16}$$

Analytic Solution

In order to solve the linearized equations, we perform the Legendre transformation:

$$\Psi(x,\theta) = \sum_{n=0}^{\infty}\Psi_n(x)P_n(\cos\theta) \tag{17}$$

$$u(x,\theta) = \sum_{n=0}^{\infty}u_n(x)P_n(\cos\theta) \tag{18}$$

$$w(x,\theta) = \sum_{n=0}^{\infty}w_n(x)P_n(\cos\theta) \tag{19}$$

$$x_s(\theta) = \sum_{n=0}^{\infty}x_{s,n}P_n(\cos\theta) \tag{20}$$

where $P_n(\cos\theta)$ is the Legendre function of order n. With these transformations, we have the following equations (see Appendix D). The continuity and the Navier-Stokes equations are:

$$x\frac{du_n}{dx} + 2u_n - n(n+1)w_n = 0 \qquad \text{for } n \geq 0 \tag{21}$$

$$\frac{3}{4}\delta_{n,1} - \frac{d\Psi_n}{dx} + \frac{d^2u_n}{dx^2} + \frac{4}{x}\frac{du_n}{dx} + \frac{2u_n}{x^2} - \frac{n(n+1)}{x^2}u_n = 0 \qquad \text{for } n \geq 0 \tag{22}$$

and

$$\frac{3}{4}\delta_{n,1} - \frac{\Psi_n}{x} - \frac{1}{x}\frac{du_n}{dx} + \frac{d^2w_n}{dx^2} + \frac{2}{x}\frac{dw_n}{dx} = 0 \qquad \text{for } n \geq 1 \tag{23}$$

where $\delta_{n,1}$ is the Kronecker's delta, so $\delta_{n,1} = 1$ for $n = 1$ and $\delta_{n,1} = 0$ for other n. The boundary conditions are written by

$$u_n = 0 \qquad \text{at} \qquad x = 1 \tag{24}$$

$$u_n = 0 \qquad \text{at} \qquad x = x_c \tag{25}$$

and

$$w_n = 0 \qquad \text{at} \qquad x = x_c \tag{26}$$

And the balance of forces on the liquid surface is given by (Appendix D):

$$a_n = \Psi_n - 2\frac{du_n}{dx} + [2 - n(n+1)]x_{n,s} \qquad \text{at } x = 1 \tag{27}$$

$$\frac{a_n}{2} = w_n - 2\frac{dw_n}{dx} \qquad \text{at } x = 1 \qquad \text{for } n \geq 1 \tag{28}$$

where $a_0 = 1/6$, $a_1 = 3/8$, $a_2 = 1/3$, $a_3 = 7/48$ and $a_n = 0$ for even $n \geq 4$, and

$$a_n = \frac{(-1)^{(n+1)/2}(n-4)!!(2n+1)}{(n+3)!!} \tag{29}$$

for odd $n \geq 5$

From these equations, we have $u_0 = x_{s0} = 0$, $\Psi_0 = 1/6$, $w_0 = -\sum_{n=1}^{\infty} w_n$, and

$$u_n = A_n x^{n+1} + B_n x^{n-1} + C_n x^{-n} + D_n x^{-n-2} \quad \text{for } n \geq 1 \tag{30}$$

as shown in Appendix D. We use the boundary conditions Equations 24, 25, and 26 to eliminate three coefficients in Equation 30 and we have (see Appendix E):

$$u_n = A_n[x^{n+1} + \alpha x^{n-1} + \beta x^{-n} - (1+\alpha+\beta)x^{-n-2}] \quad \text{for } n \geq 1 \tag{31}$$

where A_n are arbitrary constants, and α and β are given by:

$$\alpha(n, x_c) = -\frac{n(-2x_c^{2n+5} + 2x_c^{2n+3}) - x_c^{2n+5} + 3x_c^{2n+3} - 2x_c^2}{n(-2x_c^{2n+3} + 2x_c^{2n+1}) + x_c^{2n+3} + x_c^{2n+1} - 2x_c^2} \tag{32}$$

and

$$\beta(n, x_c) = \frac{1}{1-x_c^2}[(x_c^{2n+3} - 1) + \alpha(x_c^{2n+1} - 1)] \tag{33}$$

respectively. From Equation 21, we have:

$$w_n = \frac{A_n}{n(n+1)}[(n+3)x^{n-1} + (n+1)\alpha x^{n-1} + (2-n)\beta x^{-n} + n(1+\alpha+\beta)x^{-n-2}] \quad \text{for } n \geq 1 \tag{34}$$

From Equations 28 and 34, we have:

$$A_n = \frac{n(n+1)a_n}{4(\alpha+\beta)(2n+1)} \quad \text{for } n \geq 1 \tag{35}$$

From Equation 23, we have:

$$\Psi_n = \frac{3}{4}x\delta_{n,1} + \frac{a_n}{2(\alpha+\beta)(2n+1)}[(n+1)(2n+3)x^n + (2n-1)n\beta x^{-n-1}] \quad \text{for } n \geq 1 \tag{36}$$

And from Equation 27, we have:

$$x_{s,n} = \frac{a_n}{2-n(n+1)}\frac{1}{2(\alpha+\beta)(2n+1)} [2n^3 + 3n^2 - 2n - 3 + \alpha(2n^3 + 3n^2 + 5n + 2) + \beta(7n+2)] \quad \text{for } n \geq 2 \tag{37}$$

As described in section Model, we take the origin of the coordinate system so that $dr_s/d\theta = 0$ (i.e., $dx_s/d\theta = 0$) at $\theta = \pi/2$. This condition is written as $\sum_{n=0}^{\infty} x_{s,n} P_n(0) = 0$. Because $P_n(0) = 0$ for even integer n and $P_n(0) = (-1)^m(2m+1)!!/(2m)!!$ for odd integer $n = 2m+1$, we have (Appendix F):

$$x_{s,1} = -\sum_{m=1}^{\infty} x_{s,2m+1}\frac{(-1)^m(2m+1)!!}{(2m)!!} \tag{38}$$

Therefore, we have following solutions:

$$u = \sum_{n=1}^{\infty} \frac{n(n+1)a_n}{4(\alpha+\beta)(2n+1)} [x^{n+1} + \alpha x^{n-1} + \beta x^{-n} - (1+\alpha+\beta)x^{-n-2}]P_n(\cos\theta) \tag{39}$$

$$w = \sum_{n=1}^{\infty} \frac{a_n}{4(\alpha+\beta)(2n+1)} [(n+3)x^{n+1} + (n+1)\alpha x^{n-1} + (2-n)\beta x^{-n} + n(1+\alpha+\beta)x^{-n-2}] [P_n(\cos\theta) - 1] \tag{40}$$

$$\Psi = \frac{1}{6} + \frac{3}{4}x\cos\theta + \sum_{n=1}^{\infty} \frac{a_n}{2(\alpha+\beta)(2n+1)} [(n+1)(2n+3)x^n + (2n-1)n\beta x^{-n-1}] P_n(\cos\theta) \tag{41}$$

and

$$x = \sum_{m=1}^{\infty} \frac{(-1)^m (2m+1)!! a_{2m+1}}{(2m)!! 2m(2m+3)} \times \frac{16m^3 + 36m^2 + 20m + \alpha(16m^3 + 36m^2 + 34m + 12) + \beta(14m+9)}{2(\alpha+\beta)(4m+3)} \cos\theta + \sum_{m=2}^{\infty} \frac{a_m}{2 - m(m+1)} \times \frac{2m^3 + 3m^2 - 2m - 3 + \alpha(2m^3 + 3m^2 + 5m + 2) + \beta(7m+2)}{2(\alpha+\beta)(2m+1)} P_m(\cos\theta) \quad (42)$$

Forces

Heretofore, we have obtained the deformation, internal flow, and pressure distribution in the liquid shell. The internal flow and the pressure gradient exert forces on the solid core. Figure 3 depicts the geometry of forces acting on the core surface. The strengths of forces along the z-direction are obtained by integrating the force acting on a unit area of the solid core surface. The force due to the pressure gradient is given by,

$$F_p = \iint \sigma_{rr} \cos\theta dS = -2\pi r_{s0}^2 \, p_{fm} x_c^2 \int_0^{\pi} \Psi \cos\theta \sin\theta d\theta \quad (43)$$

and the force due to the friction with the internal flow is given by:

$$F_V = \iint -\sigma_{r\theta} \sin\theta dS = -2\pi r_{s0}^2 \, p_{fm} x_c^2 \int_0^{\pi} \frac{\partial^2 w}{\partial x \partial \theta} \sin^2\theta d\theta \quad (44)$$

The force due to the apparent gravitational acceleration is given by $4\pi r_c^3 \rho g_1/3$. Therefore, the force acting on the solid core is given by:

$$F = 2\pi r_{s0}^2 \, p_{fm} x_c^2 \left[\frac{x_c}{2} - \int_0^{\pi} \left(\Psi \cos\theta + \frac{\partial^2 w}{\partial x \partial \theta} \sin\theta \right) \sin\theta d\theta \right] \quad (45)$$

Properties of the Solution

Here, we examine the properties of the solution obtained in the Analytic Solution section. The velocity and the pressure distribution are displayed in Fig. 4. As can be seen from Equations 12, 13, and 14, the velocity and the pressure have solutions which are proportional to $p_{fm} r_{s0}/\eta$ and p_{fm}. The velocity has a maximum value in the vicinity of $\theta = \pi/4$ on the liquid surface and zero on the solid core surface in accordance with the boundary conditions. In the case of large core ($x_c = 0.8$), shown in panel (b), the velocity at the backside of the liquid shell is almost zero and an eddy is formed only in the front-side. The pressure distribution has the maximum value in the vicinity of $\theta = 2\pi/5$ on the liquid surface. Keeping all other conditions the same, a larger value of x_c gives a smaller velocity difference and a larger pressure difference between the front and the back of the particle. In contrast, when x_c approaches to zero (small core) or unity (thin liquid shell), the difference in pressure goes to infinite.

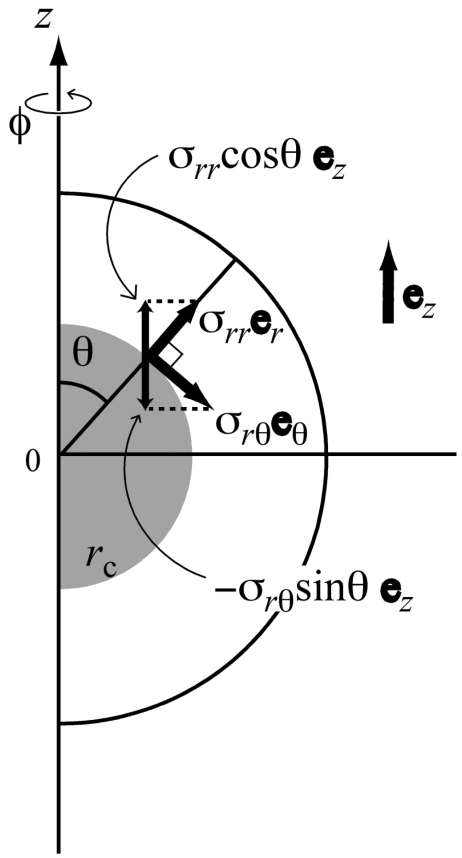

Fig. 3. Geometry of forces: $\sigma_{rr}\mathbf{e}_r$ and $\sigma_{r\theta}\mathbf{e}_\theta$ are the forces in the r and θ directions acting of the unit surface area on the solid core, and $\sigma_{rr}\cos\theta$ and $-\sigma_{r\theta}\sin\theta$ are z-components of those forces, respectively.

Figure 5 shows the surface deformation given by Equation 42. The deformation is proportional to $p_{fm} r_{s0}/T_s$ as seen from Equation 20. When $p_{fm} r_{s0}/T_s$ is fixed, larger x_c leads to a smaller deformation. On the other hand, in a limit of $x_c \to 0$, α and β behave as:

$$\alpha(0, x_c) \to 0, \beta(0, x_c) \to -1 \quad (46)$$

and

$$\alpha(n \geq 1, x_c) \to -1, \beta(n \geq 1, x_c) \to 0 \quad (47)$$

respectively. When x_{s0} is zero, terms except $n = 0$ should be

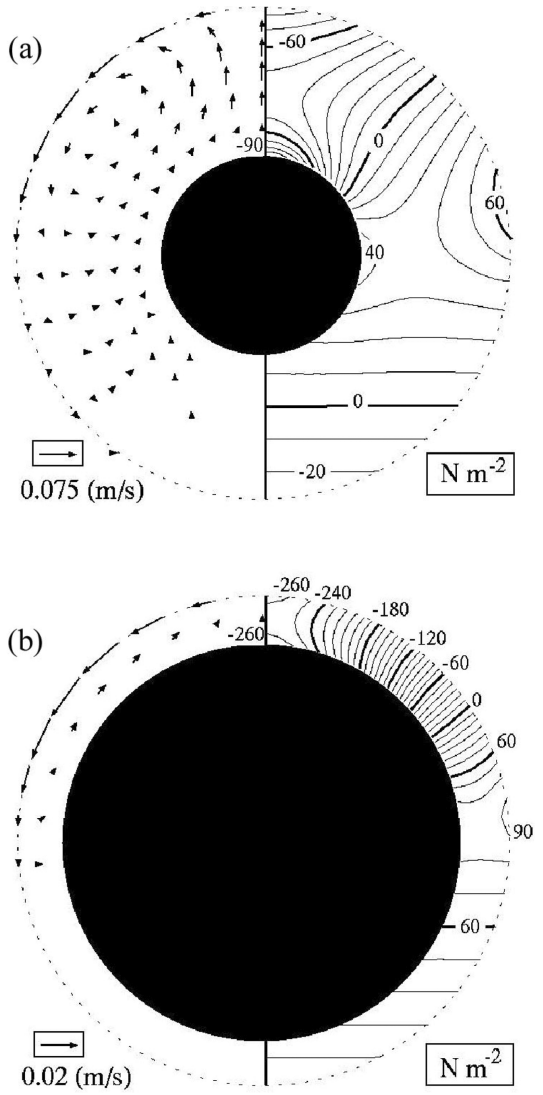

Fig. 4. The velocity (left) and the pressure (right) distributions in a liquid mantle. Parameters are $p_{fm}r_{s0}/\eta = 1$ m s^{-1} and $p_{fm} = 100$ N m^{-2}. The solid core is represented by a black circle. The ratio of the solid core to the liquid sphere x_c is (a) $x_c = 0.4$ and (b) $x_c = 0.8$, respectively.

taken into account. Then, substituting Equation 47 into Equation 42, we have the equation of the deformation in the limit of $x_c \to 0$ as:

$$x = \sum_{m=1}^{\infty} \frac{(-1)^m (7m+6)(2m+1)!!}{2m(2m+3)(4m+3)(2m)!!} a_{2m+1} \cos\theta \qquad (48)$$

$$+ \sum_{m=2}^{\infty} \frac{1}{2-m(m+1)} \left[1 + \frac{3(m+1)}{2(2m+1)}\right] a_m P_m(\cos\theta)$$

This equation is identical with the equation of deformation for a completely molten dust particle obtained by Sekiya et al. (2003). That means when we consider an extremely small solid core, the deformation of the liquid is the same with the no core case, although the velocity and the pressure

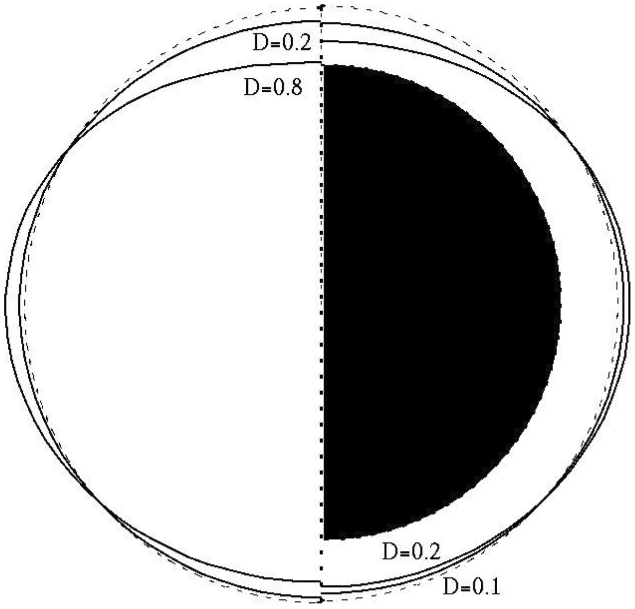

Fig. 5. The deformation of the surface with different deformation parameters $D = p_{fm}r_{s0}/T_s$ (solid curves) and the ratio of the solid core to the liquid sphere x_c (right, $x_c = 0.8$; left, x_c approaches to 0). The dotted curve represents the radius of the sphere. Black region on the right hand side corresponds to the solid core.

distribution are not exactly identical with the no core case. This difference is caused by the boundary condition at the center.

Figure 6 shows the forces on the solid core as obtained from Equation 45. All the forces increase monotonically as x_c increases. Note that the pressure gradient at the core surface increases as x_c approaches to zero. But this effect is counteracted by the effect of decay of spherical area of solid core. As a result, the total force on the solid core monotonically increases as x_c increases.

MAXIMAL SIZE OF CHONDRULES

Melting

In this study, we examine a particle that has a central solid core surrounded by a liquid mantle. This configuration is expected to be realized during the heating process in shock waves, when the following condition is satisfied:

$$t_{heat} < t_{cond} \qquad (49)$$

where t_{heat} is the time scale with which an amount of thermal energy to melt the entire dust particle is supplied by the heating mechanism, and t_{cond} is the time scale with which the heat is conducted from the surface to the center. (In reality, the melting of solid material may be controlled by kinetics [Greenwood and Hess 1994]. But we adopt a simple assumption here that the solid material starts melting when enough amount of thermal energy is supplied, so that we can

make a simple discussion. Detailed examination of melting kinetics and its influence on the stripping are left for the future work.) These time-scales are written as (Appendix G):

$$t_{heat} = \frac{\rho r_{s0}}{p_{fm} \upsilon_{rel}} L_{cond} = \quad (50)$$
$$1.35 \left(\frac{p_{fm}}{100 \text{ N m}^{-2}} \right)^{-1} \left(\frac{r_{s0}}{1 \text{ mm}} \right)$$
$$\left(\frac{\upsilon_{rel}}{10 \text{ km s}^{-1}} \right)^{-1} \left(\frac{\rho}{3.0 \times 10^3 \text{ kg m}^{-3}} \right) \text{sec}$$

and

$$t_{cond} = \frac{r_{s0}^2}{\kappa} = 0.91 \left(\frac{r_{s0}}{1 \text{ mm}} \right) \left(\frac{\kappa}{1.1 \times 10^{-6} \text{ m}^2 \text{ s}^{-1}} \right)^{-1} \text{ sec} \quad (51)$$

where $L_{cond} = 4.5 \times 10^5$ J kg^{-1} is the latent heat of melting of silicate material and κ is the heat conductivity, which is assumed to be $\kappa = 1.1 \times 10^{-6}$ m^2 s^{-1} (Stacey 1992; Podolak et al. 1993). When the time scale of heat conduction, t_{cond}, is shorter than the time scale of the heat supply t_{heat}, it is expected that the heat supplied from the dust surface transfers rapidly to the center and the entire particle reaches the same temperature. With sufficient energy, the entire particle will melt. In this case, the core-mantle structure would not be formed. In contrast, when Equation 49 is fulfilled, the supplied heat energy would not be conducted inside the particle and only the surface regions would be melted. In this case, the core-mantle structure could be formed. We can translate the condition Equation 49 into the following particle size condition:

$$r_{s0} > 1.48 \left(\frac{p_{fm}}{100 \text{ N m}^{-2}} \right)^{-1} \left(\frac{\upsilon_{rel}}{10 \text{ km s}^{-1}} \right)^{-1} \quad (52)$$
$$\left(\frac{\kappa}{1.1 \times 10^{-6} \text{ m}^2 \text{ s}^{-1}} \right) \left(\frac{\rho_d}{3.0 \times 10^3 \text{ kg m}^{-3}} \right) \text{ mm}$$

Surface melting of the particle is likely to occur when the size of the particle is large.

Stripping

Here, we discuss the motion of the solid core surrounded by the liquid mantle and estimate the possibility that the solid core leaves the liquid sphere, in other words, the liquid mantle is stripped from the solid core. In order to have such a core-mantle structure in a dust particle, the condition $t_{heat} < t_{cond}$ (Equation 49) should be satisfied. When the condition $t_{heat} < t_{cond}$ is met, the solid core would leave if a condition $t_{dyn} < t_{heat}$ is satisfied, where t_{dyn} is the dynamical time scale of the solid core to leave. Note that t_{heat} is the time scale with which the solid core would shrink and disappear by melting. When the condition $t_{dyn} < t_{heat}$ is met, the solid core can leave from the liquid mantle before disappearing.

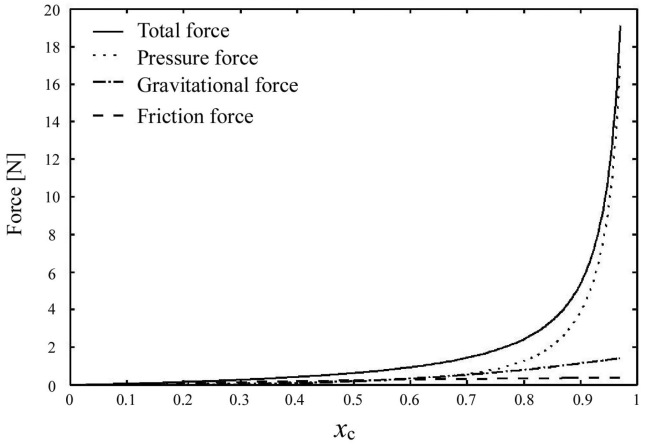

Fig. 6. Forces exert on the solid core as a function of x_c, the solid core to the liquid sphere radii ratio, in the case of $p_{fm} = 100$ N m^{-2} and $r_{s0} = 1$ mm.

We evaluate the dynamical time scale of the core's leaving from the liquid sphere. In this study, we estimate it using the acceleration time scale of the solid core t_{accel}, which is given by:

$$t_{accel} = \sqrt{\frac{2r_{s0}}{a}} = \sqrt{2r_{s0} \frac{4\pi r_c^3 \rho_d / 3}{F}} = \quad (53)$$
$$5.1 \times 10^{-3} \left(\frac{p_{fm}}{100 \text{ N m}^{-2}} \right)^{-1/2} \left(\frac{\rho_d}{3.0 \times 10^3 \text{ kg m}^{-3}} \right)$$
$$\left(\frac{r_{s0}}{1 \text{ mm}} \right) \text{ sec}$$

where $a = F/(4\pi r_c^3 \rho_d/3)$ is the acceleration due all the forces on the core (the pressure, the viscous force, and the apparent gravity). The core to liquid sphere radii ratio x_c is set to be 0.8 in Equation 53. The time scale t_{accel} given by Equation 53 expresses the time with which a point particle undergoing the constant acceleration a travels a distance r_{s0}. Obviously, the force acting on the core moving in the liquid mantle should change with time, so the time scale given by Equation 53 is not completely exact but just an order of magnitude value. Then, a condition for the liquid mantle's stripping is re-written as:

$$t_{accel} < t_{heat} \quad (54)$$

According to our simulations using the shock wave heating model by Miura and Nakamoto (2005), this condition Equation 54 is always met by chondrule-forming shock waves. Consequently, stripping of liquid mantle is expected to occur when the condition of Equation 49, i.e., Equation 52 is met.

From the discussion above, we can infer the particle size at which the stripping of molten mantle occurs. Figure 7 shows time scales t_{accel}, t_{heat}, and t_{cond} as a function of radius

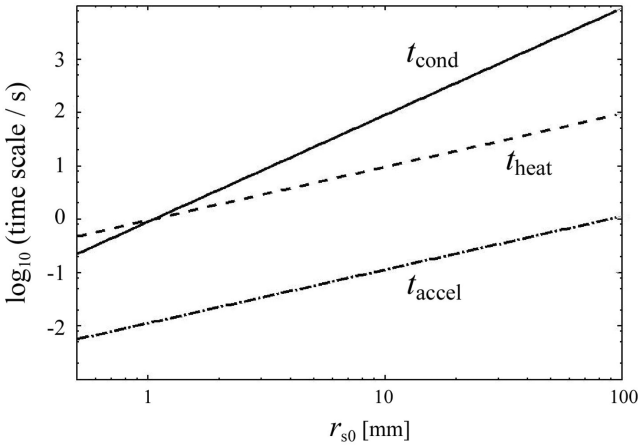

Fig. 7. Time scales as a function of radius r_0 in the case of p_{fm} = 70 N m^{-2} and υ_{rel} = 20 km s^{-1}.

r_{s0} in the case of p_{fm} = 70 N m^{-2} and υ_{rel} = 20 km s^{-1}. If r_{s0} > 1 mm, the surface melting of a particle is expected to occur, and the stripping is expected to take place. In contrast, when r_{s0} < 1 mm, the entire particle should melt without melting partially.

The critical size for stripping should be a function of p_{fm} and υ_{rel} (or equivalently, n_0 and υ_{rel}, where n_0 is the gas number density in the pre-shock region, because the gas density in the post-shock region can be related to the gas density in the pre-shock region using a shock wave heating model [e.g., Iida et al. 2001]; note that $p_{fm} = \rho_g \upsilon_{rel}^2$). Figure 8 shows a range of shock waves that can melt the dust particles (light-gray), and whether or not the stripping occurs with the shock wave; if the stripping does not take place, the shock condition is colored by a dark color. The panel (a) shows results when the initial dust radius is 2 mm. There is no dark colored region in this panel, which indicates that the stripping for 2 mm dust particles occurs in almost all the chondrule-forming shock waves. As a consequence, chondrules of 2 mm in radius is unlikely to be formed, though the final size of stripped dust particles is unknown. On the contrary, when the initial radius of the dust particle is 1 mm (panel b), it is found that chondrules of 1 mm radius can be formed without suffering stripping, if shock waves are weak (slow shock velocities and/or low gas density).

Dust particles are decelerated in the shock waves because of the gas drag. The time scale of the velocity decay is given by (Appendix G):

$$t_{stop} = \frac{4 r_{s0} \rho}{3 \rho_g \upsilon_{rel}} = 4.5 \times 10^2 \left(\frac{p_{fm}}{100\ \mathrm{N\ m^{-2}}}\right)\left(\frac{\upsilon_{rel}}{10\ \mathrm{km\ s^{-1}}}\right)\left(\frac{r_{s0}}{1\ \mathrm{mm}}\right) \mathrm{sec} \quad (55)$$

This time scale is much longer than t_{accel}, t_{heat}, and t_{cond} given by Equations 50, 51, and 53, respectively, in chondrule-forming shock waves. This suggests that the particles may be stripped over and over again in a shock wave. Indeed, according to Fig. 7, particles may finally become smaller than 1 mm. Here, we estimate the final sizes of particles, which experience the partial melting, assuming that the final radius is given so that $t_{heat} = t_{cond}$ is met. Estimated final radius as a function of the shock velocity and the gas density is shown in Fig. 9 by dashed lines. In the estimation, in order to evaluate the gas density in the post-shock region, we used the isobaric condition, which is valid for strong shock waves (Iida et al. 2001):

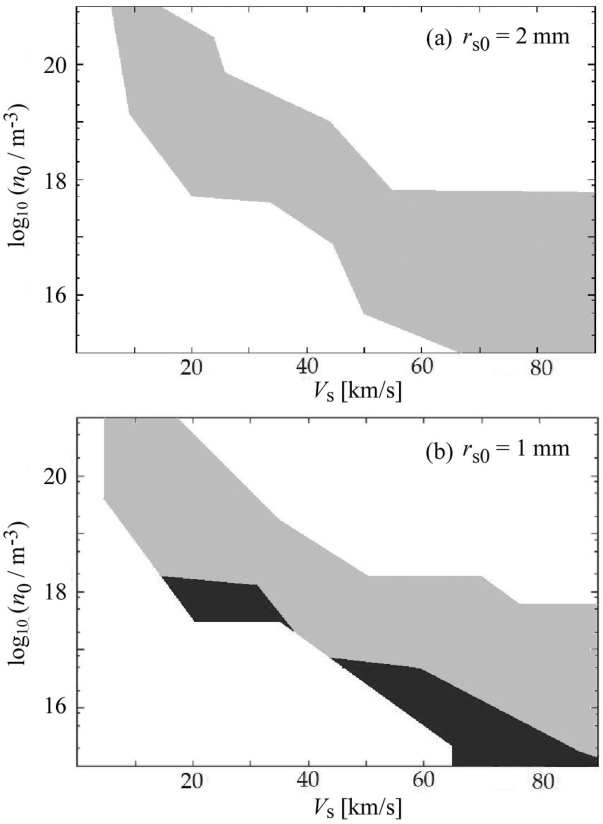

Fig. 8. Shock waves that can melt dust particles (light-gray) and shock wave in which the stripping would not take place (dark color). (a) The initial radius of dust particles is r_{s0} = 2 mm. In all the chondrule forming shock waves, the liquid mantle of dust particles is estimated to be stripped away. (b) The initial radius of dust particles is r_{s0} = 1 mm. In some weak shock waves (low shock velocity/low density), the liquid mantle seems not to be stripped off.

$$\rho_0 \upsilon_s^2 \approx \frac{\rho_{post} k T_{post}}{\mu m_p} \quad (56)$$

where ρ_0, k, μ, m_p, υ_s, ρ_{post}, and T_{post} are the gas density in the pre-shock region, Boltzmann constant, mean molecular weight, proton mass, the velocity of shock front, and the gas density and the gas temperature in the region where the particles are melting, respectively. Also, the gas temperature in the region is assumed to be T_{post} = 2,000 K (Iida et al.

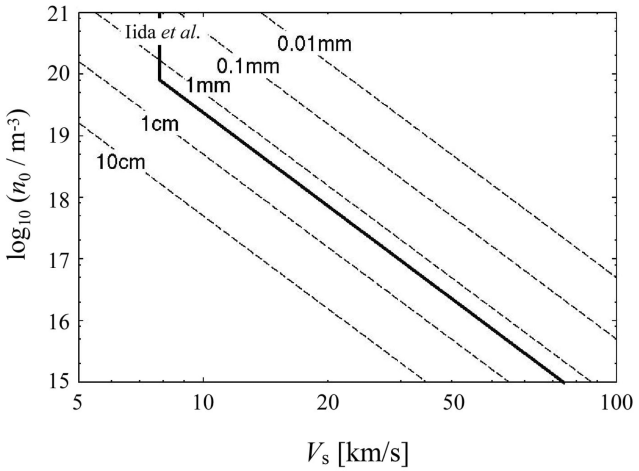

Fig. 9. The maximal size of dust particles that do not suffer from the stripping (dashed lines) as a function of the shock velocity υ_s and the pre-shock gas number density n_0. The solid line represents the boundary of shock conditions to melt the dust particle obtained by Iida et al. (2001); dust particles can melt if shock waves have υ_s and n_0 plotted in the upper-right side of the solid line. Comparing the dashed lines and the solid line, the maximal size of chondrules produced by the shock wave heating mechanism is inferred to be about 1–2 mm.

2001). From Fig. 9, it is seen that weak shock waves, i.e., slower shock velocity and/or lower pre-shock gas density, may form larger chondrules. However, the velocity of shock waves, which melt particles to form chondrules, should be larger than the critical velocity given by (Iida et al. 2001):

$$\upsilon_{s,\,crit} = \begin{cases} 7.5\ \text{km/sec} & \text{for} \quad n_0 > n_{0,\,crit} \\ 7.9\left(\dfrac{n_0}{7.4\times10^{19}\ \text{m}^{-3}}\right)^{-1/5}\left(\dfrac{T}{2000\ \text{K}}\right)^{1/5}\text{km/sec} & \text{for}\ n_0 < n_{0,\,crit} \end{cases} \tag{57}$$

and

$$n_{0,\,crit} = 7.4\times10^{19}\left(\frac{T}{2000\ \text{K}}\right)\text{m}^{-3} \tag{58}$$

This velocity condition for melting is illustrated in Fig. 9 by a solid line. Comparing the solid line and dashed lines representing different sizes, we can estimate the maximal size of chondrules, which turns out to be about a few mm. This estimated maximal size seems consistent with sizes of natural chondrules.

Porous Particle Case

In the discussion above, it is assumed that both solid and liquid materials have the same density. This assumption seems reasonable when the solid particle is dense enough. However, it is considered that the first generation precursor particles are formed through coalescence of small dust grains. The coalescence of dust grains would form fluffy or porous particles. So, the first generation chondrule precursors are likely to be porous particles. In this subsection, we will have a qualitative discussion on a chondrule-precursor particle that has a porous structure. We will see whether the porous structure may enhance or reduce the stripping effect.

In the porous dust particle, the density of the solid state before melting is lower than that of the liquid state. Then, the porous dust may be affected by following effects when it is melting:

1. The size of the liquid sphere after melting becomes smaller than the initial size.
2. A hydrodynamics time scale in the liquid shell should be different from that of an initially dense dust particle with the same initial size, because the radii ratio of the liquid sphere to the solid core (x_c) becomes different in the partial melting state.
3. The heat conductivity κ would be smaller than the dense particles, because the inner structure is porous.

In view of these effects, we estimate the critical size of the porous particle for stripping, which is evaluated using Equation 52, and the dynamical time scale, which is given by Equation 53. Here, we just assume that the density and the heat conductivity of the porous particle are 0.75 times that of the dense particle. Then, we find that the critical size for the stripping becomes about 0.7 times and the dynamical time scale is about 0.6 times of those of dense dust particles. Thus, in the case where chondrule precursor particles are porous, the maximal size of chondrules determined by the stripping, is expected to be smaller than the maximal size of chondrules formed from dense precursor particles. It is thought that chondrules may have experienced melting and re-solidifying a number of times, implying that second generation particles coming into the shock waves, which could be chondrules, may be dense particles. Then, the maximal size of chondrules may be determined by the stripping of the first generation porous dust particles; when porous particles melt for the first time to form chondrules by shock wave heating, they would suffer the stripping and the maximal size could be determined.

Fission versus Stripping: Totally versus Partially Molten Particles

Susa and Nakamoto (2002) examined the stability of totally molten particles in the hypersonic rarefied gas flow by considering the ram pressure from the gas flow and the surface tension of the molten dust particle. Since the surface tension is inversely proportional to the size of the dust particle, larger dust particles are likely to be destroyed by the ram pressure. The condition of the size for the fission was obtained by Susa and Nakamoto (2002) as:

$$r_0 > 48\left(\frac{p_{fm}}{100\ \mathrm{N\ m^{-2}}}\right)^{-1}\ \mathrm{mm} \quad (59)$$

The critical size for the fission is larger than the critical size for the stripping (given by Equation 52) in all the chondrule-forming shock waves. Thus, the maximal size of chondrules seems to be determined by the stripping of liquid mantle from partially molten dust particles, not by the fission of totally molten dust particles.

Applicability of Linear Solution

In general, if shock waves have large shock velocity and high gas number density in the pre-shock region (i.e., when the shock waves are strong enough), and also if the size of dust particles is large, the Reynolds number of the flow in the liquid mantle, $Re = \rho \upsilon_{max} r_{s0}/\eta$ would exceed unity and also the deformation of the molten particles would become considerable. For example, when $p_{fm} = 70$ N m^{-2}, $\upsilon_{rel} = 20$ km s^{-1}, and $x_c = 0.8$, the Reynolds number becomes $Re = 0.03$ for $r_{s0} = 0.9$ mm, $Re = 0.1$ for $r_{s0} = 1.5$ mm, $Re = 0.3$ for $r_{s0} = 3$ mm, and $Re = 1$ for $r_{s0} = 5$ mm. We cannot apply the linear solution obtained in this study to situations where the Reynolds number further exceeds unity, because the solution was obtained with assumptions that both the Reynolds number and the deformation are small enough. On the other hand, according to Equation 52, the critical strength of the shock waves, above which dust particles of a certain size would lose their partially molten mantle by the stripping, depends on the shock velocity and the pre-shock gas number density. When the strength of the shock wave is weaker than the critical one, the particles would form chondrules without suffering the stripping. Carrying out numerical simulations of the shock wave heating, we found that the critical strengths of shock waves for stripping are not strong enough to have a large Reynolds number and deformation. So, when we discuss the stripping of the partially molten dust particles, we can apply the linear solution obtained in this study. Therefore, the maximal size of chocndrules evaluated in this study using the linear solution is validated.

In this study, it has been assumed that the solid core and the liquid mantle are initially spherical and they are positioned concentrically. (This assumption might be validated some extent, because the flow in the back-side of the particle is quite small according to Fig. 4 and the back-side might be regarded as the solid state.) Also, some other assumptions and simplifications were used in order to analytically solve the hydrodynamics equations with linear approximation. Obviously, such a simplified case would be hardly realized in shock waves. A real situation should be more complicated: the initial shape of the dust particle may not be spherical, the dust particle in the shock wave would melt from its front-side, the viscosity in the melt may change spatially and temporary. And to examine such a complicated case precisely is far beyond the scope of this study. One might wonder whether this complicated reality may be realistically investigated by this simple model. However, we should note here that the simple model employed in this study should be helpful even in examining such a complicated case. The simple model can provide us with a useful analytic solution. For example, the simple model and analytic solution enabled us to estimate the maximal size of chondrules by the stripping, without carrying out huge numerical simulations or laboratory experiments. Although elaborate studies using numerical simulations and laboratory experiments should be used in future to address more realistic situations, the simple view and the analytic solution obtained in this study would be helpful even for those studies.

CONCLUSIONS

In the framework of the shock wave heating model for chondrule formation, we examined partially molten dust particles that have a solid core and a surrounding liquid mantle and estimated the maximal size of chondrules.

First, we examined the dynamics of the liquid mantle. Hydrodynamics equations for the core-mantle structure particles were solved analytically using a linear approximation. The deformation, the internal flow, the pressure distribution in the liquid mantle, and the force acting on the solid core were obtained.

Then, using these results, we estimated conditions in which the liquid mantle is stripped off from the solid core. To explore the stripping condition, three time scales (heating, conduction, and dynamical) were compared each other. It was found that the stripping takes place, if both $t_{heat} < t_{cond}$ and $t_{dyn} < t_{heat}$ are satisfied: the condition $t_{heat} < t_{cond}$ represents case where the partial melting and the core-mantle structure were realized in the heating phase of the shock wave heating process. The condition $t_{dyn} < t_{heat}$ means that the solid core can leave from the liquid sphere before the solid core disappearing by melting. Combining the condition for the stripping and numerical simulations of shock waves, it was found that the stripping is expected to take place before the entire dust particle melts, when the dust initial radius is larger than about 1 or 2 mm. Thus, chondrules larger than about 1–2 mm are not likely to be formed by the shock wave heating mechanism. It was also found that the stripping of the liquid mantle is more likely to occur than the fission of totally molten dust particles. Therefore, the maximal size of chondrules seems to be determined not by the fission, but by the stripping of the liquid mantle from the partially molten dust particles in the shock waves. This maximal size, about 1–2 mm, seems consistent with sizes of natural chondrules.

Acknowledgments–Authors would like to thank Prof. M. Umemura for helpful discussion. They also would like to thank Dr. K. Liffmann and an anonymous reviewer for their critical comments and suggestions for the original

manuscript. They were quite helpful to improve the manuscript. T.N. was supported by Grant-in-Aid for Young Scientists (B) (14740284) of Japan Society for the Promotion of Science, and University of Tsukuba Research Project. H.M. was supported by the Research Fellowship of the Japan Society for the Promotion of Science for Young Scientists.

Editorial Handling— Dr. Edward Scott

REFERENCES

Boss A. P. 1996. A concise guide to chondrule formation models. In *Chondrules and the protoplanetary disk*, edited by Hewins R. H., Jones R. H., and Scott E. R. D. Cambridge: Cambridge University Press. pp. 257–263.

Connolly H. C., Jr. and Love S. G. 1998. The formation of chondrules: Petrologic tests of the shock wave model. *Science* 280:62–67.

Greenwood J. P. and Hess P. C. 1994. Constraints on flash heating from melting kinetics. 25th Lunar and Planetary Science Conference. pp. 471–472.

Iida A., Nakamoto T., Susa H., and Nakagawa Y. 2001. A shock heating model for chondrule formation in a protoplanetary disk. *Icarus* 153:430–450.

Jones R. H., Lee T., Connolly H. C., Jr., Love S. G., and Shang H. 2000. Formation of chondrules and CAIs: Theory vs. observation. In *Protostars and planets IV*, edited by Mannings V., Boss A. P., and Russel S. S. Tucson, Arizona: The University of Arizona Press. pp. 927–962.

Landau L. D. and Lifshitz E. M. 1987. *Fluid mechanics,* 2nd edition. New York: Pergamon Press. 539 p.

Lipschutz M. M. 1969. *Theory and problems of differential geometry.* New York: McGraw-Hill Book Co.

Miura H., Nakamoto T., and Susa H. 2002. A shock-wave heating model for chondrule formation: Effects of evaporation and gas flows on dust particles. *Icarus* 160:258–270.

Miura H. and Nakamoto T. 2005. A shock-wave heating model for chondrule formation II: Minimum size of chondrule precursors. *Icarus* 175:289–304.

Murase T. and McBirney A. R. 1973. Properties of some common igneous rocks and their melts at high temperatures. *Geological Society of America Bulletin* 84:3563.

Podolak M., Prialnik D., Bunch T. E., Cassen P., and Reynolds R. 1993. Secondary processing of chondrules and refractory inclusions (CAIs) by gas-dynamic heating. *Icarus* 104:97–109.

Sekiya M., Uesugi M., and Nakamoto T. 2003. Flow in a liquid sphere moving with a hypersonic velocity in a rarefied gas: An analytic solution of linearized equations. *Progress of Theoretical Physics* 109:717–728.

Stacey F. E. 1992. *Physics of the earth,* 3rd edition. Brisbane: Brookfield Press.

Susa H. and Nakamoto T. 2002. On the maximal size of chondrules in shock wave heating model. *The Astrophysical Journal* 564: L57–L60.

Uesugi M., Sekiya M., and Nakamoto T. 2003. Deformation and internal flow of a chondrule-precursor molten sphere in a shocked nebular gas. *Earth, Planets and Space* 55:493–507.

APPENDIX A

Here we derive Equation 3. The left-hand side of Equation 3 represents the force acting on the surface of the particle due to the gas flow. The momentum flux of the gas flow, which is the momentum of the gas flow crossing a unit area perpendicular to the unit vector $\mathbf{e}_z$ per unit time, is given by $p_{fm} = \rho_{gas} \upsilon_{rel}^2$, where ρ_{gas} is the gas density and υ_{rel} is the relative velocity of the gas flow to the dust particle. (Strictly speaking, υ_{rel} should be the relative velocity between the gas flow and the liquid flow on the partially molten surface. But the velocity in the liquid mantle is much slower than that of the gas flow, which will be confirmed later. So, we ignore the velocity of the liquid motion on the surface, and we regard $\upsilon_{\rm rel}$ as the relative velocity between the velocity of the gas flow and the velocity of the center of mass of the dust particle.) The thermal and reflected velocities of gas molecules are small enough and are neglected. A unit area on the particle surface is projected to the flow direction, and its projected area becomes $(\mathbf{n} \cdot \mathbf{e}_z)$, where dot expresses the inner product of two vectors. Then, the force exerting on the surface of the sphere is given by $-(\mathbf{n} \cdot \mathbf{e}_z) p_{fm}\, \mathrm{H}[(\pi/2) - \theta]$, where $\mathrm{H}(x)$ is the step function whose values are unity and zero for $x \geq 0$ and $x < 0$, respectively.

The viscous flow in the particle causes the viscous force. The viscous force $\mathbf{f}_{vis}$ acting on the surface, which is normal to $\mathbf{n}$, is given by (e.g., Landau and Lifshitz 1987):

$$\begin{aligned} \mathbf{f}_{vis} &= (f_r, f_\theta, f_\phi) = \\ &(n_r \sigma_{rr} + n_\theta \sigma_{\theta r}, n_r \sigma_{r\theta} + n_\theta \sigma_{\theta\theta}, 0) = \\ &n_r \sigma_{rr} \mathbf{e}_r + n_\theta \sigma_{\theta r} \mathbf{e}_r + n_r \sigma_{r\theta} \mathbf{e}_\theta + n_\theta \sigma_{\theta\theta} \mathbf{e}_\theta \end{aligned} \tag{60}$$

And the stress tensor is given by (e.g., Landau and Lifshitz 1987):

$$\sigma_{rr} = -p + 2\eta \frac{\partial \upsilon_r}{\partial r} \tag{61}$$

$$\sigma_{\theta\theta} = -p + 2\eta \left(\frac{1}{r} \frac{\partial \upsilon_\theta}{\partial \theta} + \frac{\upsilon_r}{r} \right) \tag{62}$$

$$\sigma_{r\theta} = \sigma_{\theta r} = \eta \left(\frac{1}{r} \frac{\partial \upsilon_r}{\partial \theta} + \frac{\partial \upsilon_\theta}{\partial r} - \frac{\upsilon_\theta}{r} \right) \tag{63}$$

where p is the pressure and η is the viscosity.

The surface tension is denoted by T_s. The principal radii of curvature are given by (see Appendix B):

$$\frac{1}{R_\theta} = \frac{r_s^2 - r_s \dfrac{d^2 r_s}{d\theta^2} + 2\left(\dfrac{dr_s}{d\theta}\right)^2}{\left[r_s^2 + \left(\dfrac{dr_s}{d\theta}\right)^2 \right]^{3/2}} \tag{64}$$

and

$$\frac{1}{R_\phi} = \frac{1-\frac{1}{r_s}\frac{dr_s}{d\theta}\cot\theta}{\left[r_s^2+\left(\frac{dr_s}{d\theta}\right)^2\right]^{1/2}} \quad (65)$$

Finally, combining these terms, we have Equation 3.

APPENDIX B

Here we obtain the mean curvature. The unit tangential vectors of the surface are given by:

$$\mathbf{t}_\theta = \frac{\frac{\partial \mathbf{r}_s}{\partial\theta}}{\left|\frac{\partial \mathbf{r}_s}{\partial\theta}\right|} = \frac{\frac{dr_s}{d\theta}\mathbf{e}_r + r_s\mathbf{e}_\theta}{\left[r_s^2+\left(\frac{dr_s}{d\theta}\right)^2\right]^{1/2}} \quad (66)$$

and

$$\mathbf{t}_\phi = \frac{\frac{\partial \mathbf{r}_s}{\partial\phi}}{\left|\frac{\partial \mathbf{r}_s}{\partial\phi}\right|} = \mathbf{e}_\phi \quad (67)$$

Then, the unit normal vector of the surface is given by:

$$\mathbf{n} = n_r\mathbf{e}_r + n_\theta\mathbf{e}_\theta = \mathbf{t}_\theta \times \mathbf{t}_\phi = \frac{r_s\mathbf{e}_r - \frac{dr_s}{d\theta}\mathbf{e}_\theta}{\left[r_s^2+\left(\frac{dr_s}{d\theta}\right)^2\right]^{1/2}} \quad (68)$$

The mean curvature, which is an average of principal radii of curvature, is given by (e.g., Lipshutz 1969):

$$\frac{1}{2}\left(\frac{1}{R_{max}}+\frac{1}{R_{min}}\right) = \frac{1}{2}\left|\frac{g_{\phi\phi}h_{\theta\theta}-2g_{\theta\phi}h_{\theta\phi}+g_{\theta\theta}h_{\phi\phi}}{g_{\theta\theta}g_{\phi\phi}-g_{\theta\phi}^2}\right| \quad (69)$$

where R_{max} and R_{min} are principal radii and:

$$g_{\theta\theta} \equiv \left|\frac{\partial \mathbf{r}_s}{\partial\theta}\right|^2, g_{\phi\phi} \equiv \left|\frac{\partial \mathbf{r}_s}{\partial\phi}\right|^2, g_{\theta\phi} \equiv \frac{\partial \mathbf{r}_s}{\partial\theta}\cdot\frac{\partial \mathbf{r}_s}{\partial\theta}, \quad (70)$$
$$h_{\theta\theta} \equiv \frac{\partial^2 \mathbf{r}_s}{\partial\theta^2}\cdot\mathbf{n}, h_{\phi\phi} \equiv \frac{\partial^2 \mathbf{r}_s}{\partial\phi^2}\cdot\mathbf{n},$$
$$\text{and } h_{\theta\phi} \equiv \frac{\partial^2 \mathbf{r}_s}{\partial\theta\partial\phi}\cdot\mathbf{n}$$

Since the unit normal vector and vectors in the tangential plane are perpendicular to each other, we have:

$$\frac{\partial \mathbf{r}_s}{\partial\theta}\cdot\mathbf{n} = 0 \quad (71)$$

and

$$\frac{\partial \mathbf{r}_s}{\partial\phi}\cdot\mathbf{n} = 0 \quad (72)$$

By differentiating both sides of Equations 71 and 72 with θ and ϕ, we have:

$$\frac{\partial^2 \mathbf{r}_s}{\partial\theta^2}\cdot\mathbf{n} + \frac{\partial \mathbf{r}_s}{\partial\theta}\cdot\frac{\partial \mathbf{n}}{\partial\theta} = 0 \quad (73)$$

$$\frac{\partial^2 \mathbf{r}_s}{\partial\phi^2}\cdot\mathbf{n} + \frac{\partial \mathbf{r}_s}{\partial\phi}\cdot\frac{\partial \mathbf{n}}{\partial\phi} = 0 \quad (74)$$

and

$$\frac{\partial^2 \mathbf{r}_s}{\partial\theta\partial\phi}\cdot\mathbf{n} + \frac{\partial \mathbf{r}_s}{\partial\theta}\cdot\frac{\partial \mathbf{n}}{\partial\phi} = 0 \quad (75)$$

Using Equations 73, 74, and 75, we have:

$$h_{\theta\theta} = \frac{\partial^2 \mathbf{r}_s}{\partial\theta^2}\cdot\mathbf{n} = -\frac{\partial \mathbf{r}_s}{\partial\theta}\cdot\frac{\partial \mathbf{n}}{\partial\theta}, \quad (76)$$
$$h_{\phi\phi} = \frac{\partial^2 \mathbf{r}_s}{\partial\phi^2}\cdot\mathbf{n} = -\frac{\partial \mathbf{r}_s}{\partial\phi}\cdot\frac{\partial \mathbf{n}}{\partial\phi},$$
$$\text{and } h_{\theta\phi} = \frac{\partial^2 \mathbf{r}_s}{\partial\theta\partial\phi}\cdot\mathbf{n} = -\frac{\partial \mathbf{r}_s}{\partial\theta}\cdot\frac{\partial \mathbf{n}}{\partial\phi}$$

Thus, the mean curvature is written as:

$$\frac{1}{2}\left(\frac{1}{R_{max}}+\frac{1}{R_{min}}\right) = \frac{1}{2}\left|\frac{h_{\theta\theta}}{g_{\theta\theta}}+\frac{h_{\phi\phi}}{g_{\phi\phi}}\right| = \quad (77)$$
$$\frac{1}{2}\left|\frac{-\frac{\partial \mathbf{r}_s}{\partial\theta}\cdot\frac{\partial \mathbf{n}}{\partial\theta}}{\frac{\partial \mathbf{r}_s}{\partial\theta}\cdot\frac{\partial \mathbf{r}_s}{\partial\theta}}+\frac{-\frac{\partial \mathbf{r}_s}{\partial\phi}\cdot\frac{\partial \mathbf{n}}{\partial\phi}}{\frac{\partial \mathbf{r}_s}{\partial\phi}\cdot\frac{\partial \mathbf{r}_s}{\partial\phi}}\right|$$

since $g_{\theta\phi} = 0$ (see Equations 66, 67, and 70). And using Equation 68, we can obtain:

$$\frac{\frac{\partial \mathbf{r}_s}{\partial\theta}\cdot\frac{\partial \mathbf{n}}{\partial\theta}}{\frac{\partial \mathbf{r}_s}{\partial\theta}\cdot\frac{\partial \mathbf{r}_s}{\partial\theta}} = \frac{r_s^2 - r_s\frac{d^2r_s}{d\theta^2}+2\left(\frac{dr_s}{d\theta}\right)^2}{\left[r_s^2+\left(\frac{dr_s}{d\theta}\right)^2\right]^{3/2}} \quad (78)$$

and

$$\frac{\frac{\partial \mathbf{r}_s}{\partial\phi}\cdot\frac{\partial \mathbf{n}}{\partial\phi}}{\frac{\partial \mathbf{r}_s}{\partial\phi}\cdot\frac{\partial \mathbf{r}_s}{\partial\phi}} = \frac{1-\frac{1}{r_s}\frac{dr_s}{d\theta}\cot\theta}{\left[r_s^2+\left(\frac{dr_s}{d\theta}\right)^2\right]^{1/2}} \quad (79)$$

Therefore, by defining the principal radii of curvature as:

$$\frac{1}{R_\theta} = \frac{r_s^2 - r_s\dfrac{d^2 r_s}{d\theta^2} + 2\left(\dfrac{dr_s}{d\theta}\right)^2}{\left[r_s^2 + \left(\dfrac{dr_s}{d\theta}\right)^2\right]^{3/2}} \tag{80}$$

and

$$\frac{1}{R_\phi} = \frac{1 - \dfrac{1}{r_s}\dfrac{dr_s}{d\theta}\cot\theta}{\left[r_s^2 + \left(\dfrac{dr_s}{d\theta}\right)^2\right]^{1/2}} \tag{81}$$

we have the mean curvature as:

$$\frac{1}{2}\left(\frac{1}{R_{max}} + \frac{1}{R_{min}}\right) = \frac{1}{2}\left(\frac{1}{R_\theta} + \frac{1}{R_\phi}\right) \tag{82}$$

Note that numerators in Equations 80 and 81 are positive if the deformation is small enough.

APPENDIX C

Equations 1 and 2 are re-written by:

$$\upsilon_r = 0 \tag{83}$$

$$\upsilon_\phi = 0 \tag{84}$$

and

$$\upsilon_{r1} = 0 \tag{85}$$

at $r = r_{s0}$ by neglecting second and higher order terms. Since $r_s = r_{s0} + r_{s1}$, r_{s0} is constant, and $r_{s0} \gg |r_{s1}|$, we have:

$$\frac{\partial r_s}{\partial\theta} = \frac{\partial r_{s1}}{\partial\theta}$$

$$r_s^2 \approx r_{s0}^2(1 + 2r_{s1}/r_{s0})$$

$$r_s^2 + (dr_{s1}/d\theta)^2 \approx r_{s0}^2(1 + 2r_{s1}/r_{s0})$$

and

$$[r_s^2 + (dr_{s1}/d\theta)^2]^{-3/2} \approx r_{s0}^{-3}(1 - 3r_{s1}/r_{s0})$$

Neglecting second and higher order terms and using these expressions, Equation 7 is re-written by:

$$\frac{1}{R_\theta} = \frac{1}{r_{s0}} - \frac{1}{r_{s0}^2}\left(r_{s1} + \frac{d^2 r_{s1}}{d\theta^2}\right) \tag{86}$$

at $r = r_{s0}$, because

$$\frac{r_s^2 - r_s\dfrac{d^2 r_s}{d\theta^2} + 2\left(\dfrac{dr_s}{d\theta}\right)^2}{\left[r_s^2 + \left(\dfrac{dr_s}{d\theta}\right)^2\right]^{3/2}}$$

$$\approx r_{s0}^2\left[1 + 2\frac{r_{s1}}{r_{s0}} - \frac{1}{r_{s0}}\frac{d^2 r_{s1}}{d\theta^2}\right]\cdot\frac{1}{r_{s0}^3}\left(1 - 3\frac{r_{s1}}{r_{s0}}\right)$$

Similarly, equation (8) is re-written by:

$$\frac{1}{R_\phi} = \frac{1}{r_{s0}} - \frac{1}{r_{s0}^2}\left(r_{s1} + \frac{dr_{s1}}{d\theta}\cot\theta\right) \tag{87}$$

at $r = r_{s0}$. From these equations, Equation 3 is written by:

$$-\cos^2\theta\mathbf{H}\left(\frac{\pi}{2} - \theta\right)p_{fm1} = -p_1 + 2\eta\frac{\partial v_{r1}}{\partial r} \tag{88}$$

$$-\frac{T_s}{r_{s0}^2}\left(2r_{s1} + \frac{\partial^2 r_{s1}}{\partial\theta^2} + \cot\theta\frac{\partial r_{s1}}{\partial\theta}\right)$$

and

$$\sin\theta\cos\theta\mathbf{H}\left(\frac{\pi}{2} - \theta\right)p_{fm1} = \eta\left(\frac{\partial v_{\theta 1}}{\partial r} - \frac{v_{\theta 1}}{r_{s0}}\right) \tag{89}$$

at $r = r_{s0}$. By using Eqsuations 15 through 20, Equations 9, 10, and 11 and above equations are re-written as:

$$x\frac{\partial u}{\partial x} + 2u + \frac{\partial^2 w}{\partial\theta^2} + \cot\theta\frac{\partial w}{\partial\theta} = 0 \tag{90}$$

$$\frac{3}{4}\cos\theta - \frac{\partial\Psi}{\partial x} + \frac{\partial^2 u}{\partial x^2} + \frac{4}{x}\frac{\partial u}{\partial x} + \frac{2u}{x^2} + \frac{1}{x^2}\left(\frac{\partial^2 u}{\partial\theta^2} + \cot\theta\frac{\partial u}{\partial\theta}\right) = 0 \tag{91}$$

$$\frac{3}{4}(\cos\theta - 1) - \frac{1}{x}(\Psi - \Psi|_{\theta=0}) - \tag{92}$$

$$\frac{1}{x}\left(\frac{\partial u}{\partial x} - \left.\frac{\partial u}{\partial x}\right|_{\theta=0}\right) + \left(\frac{\partial^2 w}{\partial x^2} - \left.\frac{\partial^2 w}{\partial x^2}\right|_{\theta=0}\right) +$$

$$\frac{2}{x}\left(\frac{\partial w}{\partial x} - \left.\frac{\partial w}{\partial x}\right|_{\theta=0}\right) = 0$$

$$u = 0 \quad \text{at} \quad x = x_c \tag{93}$$

$$w = 0 \quad \text{at} \quad x = x_c \tag{94}$$

$$u = 0 \quad \text{at} \quad x = 1 \tag{95}$$

$$\cos^2\theta \mathbf{H}\left(\frac{\pi}{2}-\theta\right) = \Psi - 2\frac{\partial u}{\partial x} + 2x_s + \frac{\partial^2 x_s}{\partial\theta^2} + \cot\theta\frac{\partial x_s}{\partial\theta} \quad \text{at} \quad x = 1 \tag{96}$$

and

$$\frac{1}{2}\left[1-\cos^2\theta\mathbf{H}\left(\frac{\pi}{2}-\theta\right)\right] = \frac{\partial w}{\partial x} - w - \left(\frac{\partial w}{\partial x} - w\right)_{\theta=0} \quad \text{at} \quad x = 1 \tag{97}$$

Equations 92 and 97 are obtained by neglecting higher order terms in Equations 11 and 89, and integrating with respect to θ. The volume of the sphere is given by:

$$V = 2\pi\iint r^2 dr\sin\theta d\theta = \frac{4\pi r_{s0}^3}{3} + 2\pi r_{s0}^2\int_{-1}^{1} r_{s1}\, d\xi \tag{98}$$

where $\xi = \cos\theta$. We assume that the volume of the sphere is conserved, thus:

$$\int_{-1}^{1} x_s d\xi = 0 \tag{99}$$

APPENDIX D

The Legendre transform of the term including the step function is written:

$$\cos^2\theta\mathbf{H}\left(\frac{\pi}{2}-\theta\right) = \sum_{n=0}^{\infty} a_n P_n(\cos\theta) \tag{100}$$

where

$$a_n = \left(n+\frac{1}{2}\right)\int_0^1 \xi^2 P_n(\xi) d\xi \tag{101}$$

Calculating this integral, we have $a_0 = 1/6$, $a_1 = 3/8$, $a_2 = 1/3$, $a_3 = 7/48$, $a_n = 0$ for $n \geq 4$, and

$$a_n = \frac{(-1)^{(n+1)/2}(n-4)!!(2n+1)}{(n+3)!!} \quad \text{for} \quad \text{odd } n \geq 5 \tag{102}$$

Substituting $\theta = 0$ in Equation 100, we have

$$\sum_{n=0}^{\infty} a_n = 1 \tag{103}$$

From the property of the Legendre function, we have:

$$\left[\frac{d^2}{d\theta^2} + \cot\theta\frac{d}{d\theta} + n(n+1)\right]P_n(\cos\theta) = 0 \tag{104}$$

Substituting these equations into Equations 92 through 99, we have following equations:

$$x\frac{du_n}{dx} + 2u_n - n(n+1)w_n = 0 \quad \text{for} \quad n \geq 0 \tag{105}$$

$$\frac{3}{4}\delta_{n,1} - \frac{d\Psi_n}{dx} + \frac{d^2u_n}{dx^2} + \frac{4}{x}\frac{du_n}{dx} + \frac{2u_n}{x^2} - \frac{n(n+1)}{x^2}u_n = 0 \quad \text{for} \quad n \geq 0 \tag{106}$$

$$-\frac{3}{4} + \sum_{m=1}^{\infty}\left[\frac{\Psi_m}{x} + \frac{1}{x}\frac{du_m}{dx} - \frac{d^2w_m}{dx^2} - \frac{2}{x}\frac{dw_m}{dx}\right] = 0 \tag{107}$$

$$\frac{3}{4}\delta_{n,1} - \frac{\Psi_n}{x} - \frac{1}{x}\frac{du_n}{dx} + \frac{d^2w_n}{dx^2} + \frac{2}{x}\frac{dw_n}{dx} = 0 \quad \text{for} \quad n \geq 1 \tag{108}$$

$$u_n = 0 \quad \text{at} \quad x = 1 \tag{109}$$

$$u_n = 0 \quad \text{at} \quad x = x_c \tag{110}$$

$$w_n = 0 \quad \text{at} \quad x = x_c \tag{111}$$

$$a_n = \Psi_n - 2\frac{du_n}{dx} + [2 - n(n+1)]x_{s,n} \quad \text{at} \quad x = 1 \tag{112}$$

$$\frac{1}{2}(a_0 - 1) = \sum_{n=1}^{\infty}\left(w_n - \frac{dw_n}{dx}\right) \quad \text{at} \quad x = 1 \tag{113}$$

$$\frac{a_n}{2} = w_n - \frac{dw_n}{dx} \quad \text{at} \quad n \geq 1 \tag{114}$$

From Equation 105 with $n = 0$, we have $x^2u_0 =$ constant, and we get $u_0 = 0$ from Equation 109. From Equation 106, we have $\Psi_0 =$ constant. From Equation 99, we have $x_{s0} = 0$. Thus, we have $\Psi_0 = 1/6$ from Equation 113 for $n = 0$. Calculating $d\Psi_n/dx$ from Equation 108, and using Equation 105 and 106, we have:

$$x^4\frac{d^4u_n}{dx^4}+8x^3\frac{d^3u_n}{dx^3}+[12-2n(n+2)]x^2\frac{d^2u_n}{dx^2}-4n(n+1)x\frac{du_n}{dx} \quad (115)$$

$$-n(n+1)[2-n(n+1)]u_n=0 \qquad \text{for} \qquad n\geq 1$$

Assuming the solution has a form $u_n \propto x^{\lambda}$ and substituting it toEquation 115, we have:

$$\lambda(\lambda-1)(\lambda-2)(\lambda-3)+8\lambda(\lambda-1)(\lambda-2)+ \quad (116)$$
$$[12-2n(n+1)]\lambda(\lambda-1)-4n(n+1)\lambda-$$
$$n(n+1)[2-n(n+1)]=0 \qquad \text{for} \qquad n\geq 1$$

Solving these equations, we obtain $\lambda = n+1, n-1, -n, -n-2$. Thus:

$$u_n = A_n x^{n+1}+B_n x^{n-1}+C_n x^{-n}+D_n x^{-n-2} \quad (117)$$
$$\text{for} \qquad n\geq 1$$

where A_n, B_n, C_n, and D_n are constants.

APPENDIX E

Here, we derive Equations 31, 32, and 33. Using Equations 21 and 30, we have an expression for w_n as:

$$w_n = \frac{1}{n(n+1)}\left[x\frac{du_n}{dx}+2u_n\right] = \frac{1}{n(n+1)} \quad (118)$$
$$[(n+3)A_n x^{n+1}+(n+1)B_n x^{n-1}+$$
$$(2-n)C_n x^{-n}-nD_n x^{-n-2}]$$

Then, substituting the Expression 30 into the boundary condition (24), we have $A_n+B_n+C_n+D_n=0$, thus:

$$D_n = -A_n-B_n-C_n \quad (119)$$

Similarly, from Equations 25 and 30, we have

$$A_n x_c^{n+1}+B_n x_c^{n-1}+C_n x_c^{-n}+D_n x_c^{-n-2}=0$$

and using Equation 119, then:

$$C_n = \frac{1}{1-x_c^2}[(x_c^{2n+3}-1)A_n+(x_c^{2n+1}-1)B_n] \quad (120)$$

And using Equation 26, 119, and 120, we have:

$$(n+3)A_n x_c^{n+1}+(n+1)B_n x_c^{n-1}+ \quad (121)$$
$$(2-n)x_c^{-n}\frac{1}{1-x_c^2}[(x_c^{2n+3}-1)A_n+$$
$$(x_c^{2n+1}-1)B_n]-nx_c^{-n-2}$$
$$\left[-A_n-B_n-\frac{1}{1-x_c^2}\{(x_c^{2n+3}-1)A_n+(x_c^{2n+1}-1)B_n\}\right]$$
$$=0$$

This Equation 121 can be re-written as:

$$A_n[2n(-x_c^{2n+5}+x_c^{2n+3})- \quad (122)$$
$$x_c^{2n+5}+3x_c^{2n+3}-2x_c^2]+$$
$$B_n[2n(-x_c^{2n+3}+x_c^{2n+1})+$$
$$x_c^{2n+3}+x_c^{2n+1}-2x_c^2]=0$$

Thus,

$$\alpha(n,x_c)\equiv\frac{B_n}{A_n}= \quad (123)$$
$$-\frac{2n(-x_c^{2n+5}+x_c^{2n+3})-x_c^{2n+5}+3x_c^{2n+3}-2x_c^2}{2n(-x_c^{2n+3}+x_c^{2n+1})+x_c^{2n+3}+x_c^{2n+1}-2x_c^2}$$

where α is a ratio between A_n and B_n, and Equation 123 becomes Equation 32. Also, from Equations 120 and 123, a ratio between A_n and C_n, which is defined as β, is given by:

$$\beta(n,x_c)\equiv\frac{C_n}{A_n} = \frac{1}{1-x_c^2}[(x_c^{2n+3}-1)+\alpha(x_c^{2n+1}-1)] \quad (124)$$

Equation 124 corresponds to Equation 33. And using Equations 119, 123, and 124, we have:

$$D_n = -A_n-\alpha A_n-\beta A_n \quad (125)$$

Finally, substituting Equations 123, 124, and 125 into Equations 30, we have Equation 31.

APPENDIX F

As described in section Linear Approximation and Non-Dimensional Variables, we have:

$$\sum_{n=0}^{\infty} x_{s,n}P_n(0)=0 \quad (126)$$

This summation can be re-written as:

$$\sum_{m=0}^{\infty} x_{s,2m}P_{2m}(0)+\sum_{m=0}^{\infty} x_{s,2m+1}P_{2m+1}(0)=0 \quad (127)$$

where the first and second terms correspond to the even integer n and odd integer n in the summation of Equation 126, respectively. And $P_{2m}(0)=0$ for integer $m\geq 0$. Thus, Equation 127 becomes:

$$\sum_{m=0}^{\infty} x_{s,2m+1}P_{2m+1}(0) \quad (128)$$
$$= x_{s,1}P_1(0)+\sum_{m=1}^{\infty} x_{s,2m+1}P_{2m+1}(0)=0$$

Since $P_{2m+1}(0)=(-1)^m(2m+1)!!/(2m)!!$ and $P_1(0)=1$, we have:

$$x_{s,1} + \sum_{m=1}^{\infty} x_{s,2m+1} \frac{(-1)^m (2m+1)!!}{(2m)!!} = 0 \tag{129}$$

And from this Equation 129, we have Equation 38.

APPENDIX G

In this appendix, expressions of heating time scale, conduction time scale, and stopping time are given.

Injected energy from the gas flow to the particle per unit time is given by $\pi r_s^2 \rho_{gas} \upsilon_{rel}^3$. The required energy to melt the particle completely at the melting temperature is evaluated to be $\frac{4\pi}{3} r_s^3 \rho L_{melt}$.

Thus, the heating time scale, t_{heat}, to melt the particle is estimated by equating

$$\pi r_s^2 \rho_{gas} \upsilon_{rel}^3 \cdot t_{heat} = \frac{4\pi}{3} r_s^3 \rho L_{melt} \tag{130}$$

and neglecting some order of unity factors as:

$$t_{heat} = \frac{r_s \rho}{\rho_{gas} \upsilon_{rel}^3} L_{melt} = \frac{r_s \rho}{p_{fm} \upsilon_{rel}} L_{melt} \tag{131}$$

The heat conduction equation is given by (e.g., Landau and Lifshitz 1987):

$$\frac{\partial T}{\partial t} = \kappa \frac{\partial^2 T}{\partial x^2} \tag{132}$$

where x is the spatial distance. Evaluating derivatives by divisions and substituting $\Delta t \approx t_{cond}$ and $\Delta x \approx r_{s0}$, we have

$$t_{cond} = \frac{r_{s0}^2}{\kappa} \tag{133}$$

The equation of motion of the particle in the post-shock region is given by:

$$\frac{4\pi r_s^3}{3} \rho \frac{d\upsilon_{rel}}{dt} = -\pi r_s^2 \rho_{gas} \upsilon_{rel}^2 \tag{134}$$

since the gas flow is the free molecular flow and the relative velocity is faster than the gas thermal velocity. Evaluating the time derivative by:

$$\frac{d\upsilon_{rel}}{dt} \approx -\frac{\upsilon_{rel}}{t_{stop}} \tag{135}$$

and using a relation $p_{fm} = \rho_{gas} \upsilon_{rel}^2$, we have:

$$t_{stop} = \frac{4 r_{s0} \rho}{3 \rho_{gas} \upsilon_{rel}} = \frac{4 r_{s0} \rho \upsilon_{rel}}{3 p_{fm}} \tag{136}$$